Sensitivity Limits of Continuous Wave Cavity Ring-Down Spectroscopy

ARTICLE *in* THE JOURNAL OF PHYSICAL CHEMISTRY A · AUGUST 2013

Impact Factor: 2.69 · DOI: 10.1021/jp406691e · Source: PubMed

2 AUTHORS, INCLUDING:

Kevin Lehmann
University of Virginia
244 PUBLICATIONS **5,864** CITATIONS

SEE PROFILE

THE JOURNAL OF PHYSICAL CHEMISTRY A

Article

pubs.acs.org/JPCA

Sensitivity Limits of Continuous Wave Cavity Ring-Down Spectroscopy

Haifeng Huang and Kevin K. Lehmann*

Department of Chemistry, University of Virginia, Charlottesville, Virginia 22904-4319, United States

ABSTRACT: An optimized nonlinear least-squares fit algorithm for data processing in cavity ring-down spectroscopy (CRDS) is discussed, which improves the calculation efficiency substantially over using a general purpose fitting package. Theoretical absorption sensitivity limits for both the detector noise and the shot noise limited situations are derived and compared with experimental results. The effect of limiting the bandwidth of detection system on ring-down signal is discussed and compared with real ring-down data. The optimal trigger level and fitting interval are obtained for continuous wave cavity ring-down spectroscopy (cw-CRDS) in both the detector noise and shot noise limits, with the resulting sensitivity in units of cm^{-1} per $(Hz^{1/2})$ derived. Interestingly, it is found that the optimized shot noise limited sensitivity in cw-CRDS method is, in principle, comparable with the ultimate sensitivity of noise-immune cavity-enhanced optical heterodyne molecular spectroscopy (NICE–OHMS).

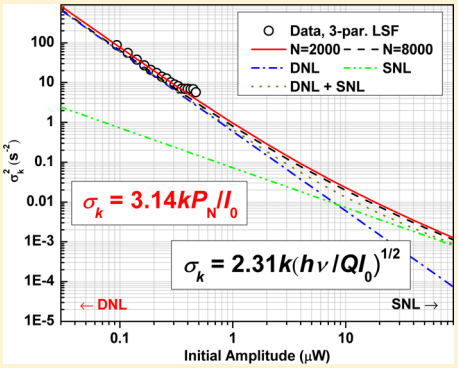

INTRODUCTION

Cavity ring-down spectroscopy (CRDS) has become a widely used method for the detection of weak absorption features in gaseous samples.[1−5] In this method, sample absorption is detected as an increase in the decay rate of light trapped in a low loss (high finesse) optical cavity.[6] While the theoretical shot-noise detection limit of the method has long been known,[7] the limit appropriate for the more common case where detector noise dominates has only recently been published.[8] Even in that case, the noise was expressed in terms of the fluctuations in the decay rate extracted from a single cavity decay transient, not in terms of noise per root Hz. Assuming that the noise in each cavity decay is statistically independent, the latter is reduced from the former by the square root of the number of decays per second that are observed, but in cw-CRDS, the rate of detected ring-down transients depends upon the trigger threshold level used to initiate an observed decay and the time interval that the cavity transmission transient is recorded. In this publication, we determine the optimal values of these parameters that are predicted to lead to the lowest possible noise per unit bandwidth and thus the highest possible sensitivity of the cw-CRDS method.

Before that, we will briefly represent an optimized nonlinear least-squares fit (LSF) algorithm for data processing in CRDS experiments and the derived theoretical sensitivity limits of CRDS method. Both have been published previously,[8] but in a book chapter that may not be available to many. Following this, we will discuss experimental results of the sensitivity with our cw-CRDS instrument and compare them with the model. Furthermore, we use this opportunity to correct a factor of 2 error that we detected in our previous work.

SENSITIVITY LIMITS OF AMPLITUDE MODULATED CW-CRDS

Consider that one observes a cw-CRDS signal as N discrete points, y_i, $i = 0...N-1$, each equally separated in time by Δt. We further assume that the input laser intensity is rapidly switched completely off when the power on the detector reaches a preset value, I_{th}. For a discussion of the effects of finite excitation light extinction, see ref 9. The detector signal as a function of time will be given by:

$$y(t) = F(t) + \varepsilon(t) = Ae^{-kt} + B + \varepsilon(t) \quad (1)$$

with $F(t)$ as the intrinsic detector signal and $\varepsilon(t)$ as the noise. $F(t)$ is treated as a single exponential decay with cavity decay rate k (or equivalently, cavity decay time $\tau = 1/k$), ring-down amplitude A, and baseline or detector offset B. In the case where $\varepsilon(t)$ is a Gaussian random variable, the optimal signal processing to extract the smallest dispersion in the cavity decay rate and thus highest absorption sensitivity is to perform a weighted LSF to the observed cavity transmission power following triggering.[8] The assumed form of $F(t)$ ignores distortion due to the finite detector and amplifier bandwidths and the finite time required to turn off the laser with sufficient attenuation.[8,9] The latter affects only the points at the very beginning of the decay and thus these data points are often ignored in the fit to retain accuracy. Additionally, we have found that a small amount of gain compression (partial

Special Issue: Terry A. Miller Festschrift

Received: July 7, 2013
Revised: August 22, 2013

   dx.doi.org/10.1021/jp406691e | J. Phys. Chem. A XXXX, XXX, XXX–XXX

saturation) of the detector/amplifier can distort the early signal, and thus we check and begin the fit only after the decay has passed below some upper limit threshold.

The LSF requires a model for the statistical properties of the noise, $\varepsilon(t)$. If the detector/amplifier is treated as a single pole, low-pass (LP) filter with 3 dB role-off at angular frequency k_f, then the noise characteristics can be shown to be[8]

$$\langle \varepsilon(t) \rangle = 0$$

$$\langle \varepsilon(t)\, \varepsilon(t') \rangle = \frac{k_f}{2} \sigma'^2 \left(\frac{t + t'}{2} \right) \exp(-k_f |t - t'|) \tag{2}$$

where $\sigma'^2(t)$ is the two sided noise power density at time t and it is assumed that it changes slowly on a time scale of $t_f = 1/k_f$ which is the noise correlation time. By two-sided, we mean that the noise spectrum is considered to run from $[-\infty, +\infty]$. We consider two contributions to σ', shot noise and detector noise, and we can write

$$\sigma'^2(t) = \frac{1}{2} \left[\frac{2h\nu}{Q} I(t) + P_N{}^2 \right] \tag{3}$$

where ν is the frequency of the light, $I(t)$ the light power imaged on the detector, Q the quantum efficiency of the detector, and P_N the optical noise equivalent power (NEP) of the detector, amplifier combination. The factor of 1/2 out front accounts for the fact that the NEP is usually defined in terms of the one-sided spectral noise density, where frequency runs from $[0, +\infty]$, and thus the spectral noise density is twice as high to account for the folding over of the frequency axis. In our previous paper,[8] we properly accounted for the shot noise (since we used the two-sided spectral noise density), but expressions with P_N should be replaced by $P_N/(2^{1/2})$. Note that we are measuring the signals in units of watts; to convert to voltage one must first multiply by the photodetector response $S(\lambda)$ (in A/W) then times the transimpedance gain of the amplifier. Here λ is the laser wavelength. The detector quantum efficiency is $Q = S(\lambda)hc/e\lambda$. The photodetector response $S(\lambda)$ or $Q(\lambda)$ is often given by manufacturers. h is the Planck constant, c is the speed of light, and e is the quantum of electric charge.

The fit to a single exponential function has three parameters: cavity decay rate k (or equivalently, cavity decay time $\tau = 1/k$), ring-down amplitude A, and baseline or detector offset B, where the latter can be treated as a constant if the baseline is very stable. The LSF to the data is in general iterative because of the nonlinear dependence of the model on k. Linearization of the equations that result from minimizing χ^2 reduces to the linear system of equations $\alpha \Delta p = \beta$. Δp is the change of fitting parameters in each cycle of iteration.[10] In the cases where either detector or shot noise dominates throughout the decay, the curvature matrix, α, (which is symmetric) can be calculated in closed form using geometric series. For the case where detector noise dominates, $\sigma'^2 = P_N{}^2/2$ for all times, and each data point has variance $\sigma^2 = k_f P_N{}^2/4$. For this constant weight fit, we have that α and β are given by:[8]

$$\alpha_{B,B} = \frac{N}{\sigma^2} \tag{4}$$

$$\alpha_{B,A} = \left(\frac{1 - a^N}{1 - a} \right) \frac{1}{\sigma^2}$$

$$\alpha_{B,k} = -A\Delta t \left(\frac{a(1 - a^N)}{(1 - a)^2} - \frac{Na^N}{1 - a} \right) \frac{1}{\sigma^2}$$

$$\alpha_{A,A} = \left(\frac{1 - a^{2N}}{1 - a^2} \right) \frac{1}{\sigma^2}$$

$$\alpha_{A,k} = -A\Delta t \left(\frac{a^2(1 - a^{2N})}{(1 - a^2)^2} - \frac{Na^{2N}}{1 - a^2} \right) \frac{1}{\sigma^2}$$

$$\alpha_{k,k} = (A\Delta t)^2 \left(\frac{2a^4(1 - a^{2N})}{(1 - a^2)^3} + \frac{a^2 - (2N + 1)a^{2N+2}}{(1 - a^2)^2} - \frac{N^2 a^{2N}}{1 - a^2} \right) \frac{1}{\sigma^2}$$

$$\beta_B = \left(\sum_i y_i - A \left(\frac{1 - a^N}{1 - a} \right) - BN \right) \frac{1}{\sigma^2} \tag{5}$$

$$\beta_A = \left(\sum_i y_i a^i - A \left(\frac{1 - a^{2N}}{1 - a^2} \right) - B \left(\frac{1 - a^N}{1 - a} \right) \right) \frac{1}{\sigma^2}$$

$$\beta_k = -A\Delta t \left(\sum_i y_i i a^i - A \left(\frac{a^2(1 - a^{2N})}{(1 - a^2)^2} - \frac{Na^{2N}}{1 - a^2} \right) - B \left(\frac{a(1 - a^N)}{(1 - a)^2} - \frac{Na^N}{1 - a} \right) \right) \frac{1}{\sigma^2}$$

where $a = \exp(-k\Delta t)$. The standard error of k in a fit to one decay transient is given by the square root of the k,k element of the covariance matrix, $\varepsilon = \alpha^{-1}$. The noise in sample absorption coefficient (which determines the sensitivity of the experiment) is the noise in k divided by the speed of light. Note that σ^2 factors out of the equation for $\Delta p = \varepsilon\beta$ but appears as a scale factor in the expression for ε. For the case of two parameters (A and k with B fixed) we can write

$$|\varepsilon| = |\alpha|^{-1} = (\alpha_{AA}\alpha_{kk} - \alpha_{A,k}^2)^{-1} \tag{6}$$

$$\varepsilon_{A,A} = |\varepsilon| \alpha_{k,k}$$

$$\varepsilon_{A,k} = -|\varepsilon| \alpha_{A,k}$$

$$\varepsilon_{k,k} = |\varepsilon| \alpha_{A,A}$$

while in the three free parameter case, we can write

$$|\varepsilon| = |\alpha|^{-1} \tag{7}$$

$$|\alpha| = \alpha_{B,B}\alpha_{AA}\alpha_{kk} + \alpha_{B,A}\alpha_{A,k}\alpha_{B,k} + \alpha_{B,k}\alpha_{B,A}\alpha_{A,k} - \alpha_{B,B}\alpha_{A,k}^2 - \alpha_{A,A}\alpha_{B,k}^2 - \alpha_{k,k}\alpha_{B,A}^2$$

$$\varepsilon_{B,B} = |\varepsilon| (\alpha_{A,A}\alpha_{k,k} - \alpha_{A,k}^2)$$

$$\varepsilon_{B,A} = |\varepsilon| (\alpha_{B,k}\alpha_{A,k} - \alpha_{B,A}\alpha_{k,k})$$

$$\varepsilon_{B,k} = |\varepsilon| (\alpha_{B,A}\alpha_{A,k} - \alpha_{B,k}\alpha_{A,A})$$

$$\varepsilon_{A,A} = |\varepsilon| (\alpha_{B,B}\alpha_{k,k} - \alpha_{B,k}^2)$$

$$\varepsilon_{A,k} = |\varepsilon| (\alpha_{B,A}\alpha_{B,k} - \alpha_{A,k}\alpha_{B,B})$$

dx.doi.org/10.1021/jp406691e | J. Phys. Chem. A XXXX, XXX, XXX−XXX

$$\varepsilon_{k,k} = |\varepsilon|(\alpha_{B,B}\alpha_{A,A} - \alpha_{B,A}^2)$$

This treatment ignores the correlation of the data due to the finite bandwidth of the detector/amplifier combination. We previously demonstrated that, for the case $k_f \gg k$, the above equations can still be used but the data variances $\sigma^2 = Gk_f{P_N}^2/4$ where the scale factor $G = \tanh^{-1}(k_f\Delta t/2)$.[8] G corrects for the fact that the effective number of "independent" data points is less than N since data points within a time of $\sim 1/k_f$ have correlated noise. Previously we have demonstrated that the optimum k_f gives $k_f\Delta t \sim 1$.[8] If the digitization rate is sufficiently fast to fully sample the detector noise spectrum (i.e., Δt is smaller than the inverse of the detector 3 dB angular frequency k_f), one can replace the true detector root-mean-square (RMS) noise σ in eqs 4 and 5 by $P_N/(2\Delta t)^{1/2}$.[8] This is because $G(k_f/4){P_N}^2 = G(k_f\Delta t/2)({P_N}^2/2\Delta t) = \xi^2({P_N}^2/2\Delta t)$, and ξ^2 is very close to one if $k_f\Delta t < 1$.[8] For nonideal sampling, the variance in k is larger than the ideal case by a factor of ξ^2. We earlier showed that in the limit $k\Delta t \ll 1$ and $Nk\Delta t \gg 1$, for the detector noise limited (DNL) case, we get the standard error in the extraction of the cavity decay rate, σ_k, from a single ring-down event as

$$\sigma_k^2 = 8k^3\Delta t(\sigma/A)^2 = 4k^3(P_N/A)^2 \quad (8)$$

This "ideal" noise applies regardless of whether the detector background is treated as fixed or a fit variable, if one observes sufficiently far into the tail of the decay. However, for a variable baseline, correlation between k and B raise the standard error in k for a finite fit interval. Plots showing how the standard error in k changes with fitting interval and digitization rate are given in our previous paper.[8] These are easily reproduced from the above expressions for $\varepsilon_{k,k}$.

For the case where shot-noise dominates, the same least-squares equations can be used with the substitutions that $a = \exp(-k\Delta t/2)$ and $\sigma = (h\nu A/Q\Delta t)^{1/2}$. This can be understood by observing that, in the shot noise case, the electric field can be viewed as having constant noise (as the intensity does in the detector noise case), and the electric field amplitude decays at half the rate as the intensity. In the shot noise limited (SNL) case,

$$\sigma_k^2 = k^3\Delta t(\sigma/A)^2 = k^3\left(\frac{h\nu}{AQ}\right) \quad (9)$$

This result was previously derived by Romanini and Lehmann.[7] As in the DNL case, we assume the shot noise spectrum limited by detector bandwidth is fully sampled. In general, the standard error in k extraction is

$$\sigma_k^2 = \xi^2k^3\left(\frac{h\nu}{AQ}\right) \quad (10)$$

If SNL data are fit with an equally weighted LSF, as appropriate for the case of DNL case, error propagation predicts that the nonoptimal weighting of the data increases the fluctuations of k such that $\xi^2 = (80/27) \approx 2.96$; that is, the fluctuations in k are about 72% higher than optimal.[8]

In our previous publication,[8] we have presented an optimized data processing algorithm in CRDS experiments which includes the above closed form expressions for both the curvature matrix α (eq 4) and vector β (eq 5) in a constant weight LSF. Calculation of the components of β requires only the calculation of three terms in a sum over data points with three floating point additions and three floating point multiplications per data point in the case of three-parameter fits. For two-parameter fits (B fixed), we have one less variable and one less sum per data point. The nonlinear LSF has quadratic convergence. With an initial fractional error of ~0.1 in k, a value within 1% of the converged value will be returned after one iteration and within ~0.01% after two iterations.[8] The latter is usually well below the noise level, σ_k. Starting values of k can be taken from the previous decay fit, or from the first data point that is a fraction of e^{-1} times the difference of the first and last point plus the last point value. In the same article, we have also reviewed other algorithms of data processing that are commonly used in CRDS experiments. Some of the discussed methods are noniterative, such as determining decay rate k by fast Fourier transform (FFT),[11] the successive integration (SI) method,[12] and corrected successive integration (CSI) method.[13] Some use analog detection methods, such as phase-shift CRDS,[14] gated integrator method,[7] and logarithm differentiator method.[15] When compared with our optimized fitting algorithm, as opposed to the use of a general-purpose Levenberg–Marquardt algorithm package,[10] those noniterative methods actually need more calculation steps and are less efficient than our LSF method. In spite of high speed, the analog methods all share the disadvantage that they provide no check for the quality of the data processing; thus they can generate nonphysical results when bad decays happen. In contrast, our optimized algorithm uses the reduced χ^2 of the fit to assess the quality of LSF,[8] and we remove fits with χ^2 over a specified threshold. This removes most "bad" decays which, for example, can arise from triggering on higher order modes, which display mode beating between the nearly degenerate transverse modes in a nominally cylindrically symmetric cavity.[16]

NOISE AND BANDWIDTH OF THE DETECTION SYSTEM

In this section we will discuss some details of noise level and bandwidth of the detection system in our cw-CRDS setup. The information is necessary when analyzing our results with the theoretical model discussed in last section. The detection system includes a detector and an A/D converter, between which a homemade antialiasing LP filter can be added.

Our detector is a room temperature InGaAs photodiode with a 0.3 mm diameter (Hamamatsu G8376-03), followed by two stages of amplification. The first stage amplifier has a transimpedance design with inverting input of an op-amp (OPA655); the second stage uses another same type of op-amp but with noninverting input. The feedback resistor R_f in the first stage amplifier is 1 MΩ. The second stage has 10 different gain settings from G0 to G9, corresponding to discrete gains 1, 2, 5, 6, 9, 10, 13, 14, 24, and 25, respectively. The total transimpedance gain of the detector is the product of both stage gains. With a scope (LeCroy 6030A), we have measured the output voltage noise level of the detector at all gain settings when it was powered by a low noise DC power supply (New Focus 0901) with the incident window covered. The noise level is defined as the standard deviation of its output voltage noise trace on a 50 Ω load. Each trace has 100 000 data points recorded in a 5 ms time period. The measured noise levels are 0.66, 0.91, 1.9, 2.2, 3.1, 3.5, 4.3, 4.6, 7.4, and 7.6 mV for G0 to G9 settings, respectively. The three lowest gain settings: 1×10^6 (G0), 2×10^6 (G1), and 5×10^6 (G2), in V/A, are mostly used in our CRDS experiments,

The detector bandwidth at different gains was measured by the impulse response method.[17] Figure 1a displays the time

dx.doi.org/10.1021/jp406691e | J. Phys. Chem. A XXXX, XXX, XXX–XXX

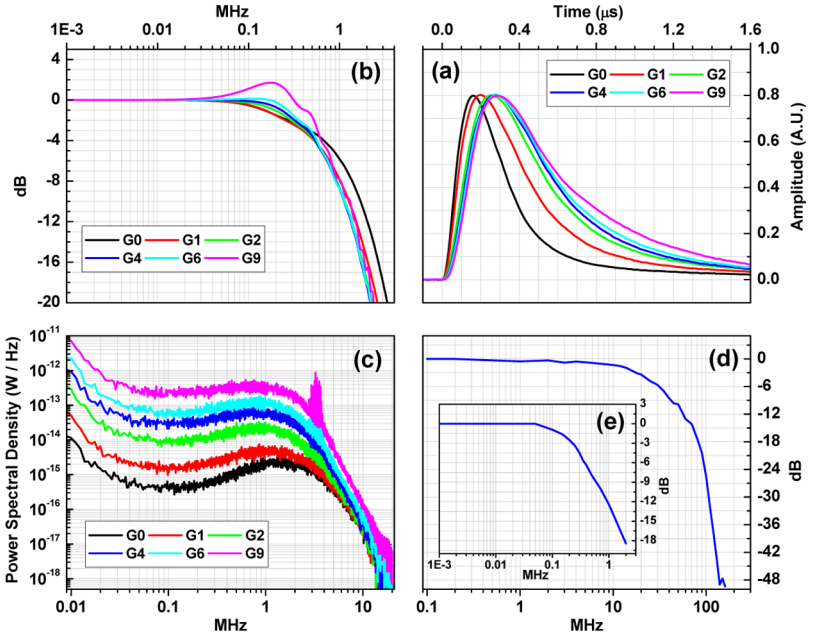

Figure 1. (a) Impulse response of the detector at gain settings G0, G1, G2, G4, G6, and G9, recorded by the scope with 50 Ω DC coupling when excited by a ns pulsed laser. All have been adjusted to the same amplitude and are well below the saturation voltage of the detector output. The trace of G0 has a full-width-half-maximum (FWHM) of 0.28 μs. (b) Fourier transform (FT) power spectra of the time traces in panel a. (c) Noise power spectra of the detector at G0, G1, G2, G4, G6, and G9 settings measured by a spectral analyzer (HP E4402B). (d) The 3 dB bandwidth of the A/D converter is about 17 MHz. (e) The 3 dB bandwidth of the antialiasing RC LP filter plus the following amplifier is measured to be 220 kHz.

traces of impulse response at G0, G1, G2, G4, G6 and G9 settings when the detector was excited by a 10 ns pulsed YAG laser (Coherent Surelite III-10). Figure 1b shows the Fourier transform (FT) power spectra of the time traces in 1a. On the other hand, the noise power spectra of the detector in Figure 1c were measured at the same detector gain settings by a spectral analyzer (HP E4402B, spectral range 9 kHz to 3 GHz). For clarity, the traces of G3, G5, G7, and G8 are not displayed in Figure 1, which are very close to those of G2, G4, G6, and G9, respectively. From panel 1a, the FWHM of the time traces increases with detector gain. The 3 dB bandwidths from impulse response method are 473, 396, 420, 445, 445, 501, 486, 482, 579, and 573 kHz for G0 to G9 settings, respectively. The spectra of G8 (not shown) and G9 show a clear gain peak near 150 kHz, which leads to an increase of 3 dB bandwidth. The reason for this gain peak is unknown to us.

The noise spectra in Figure 1c show excess low frequency noise below 0.03 MHz and a 3 dB bandwidth about 2−3 MHz, about 4−6 times larger than the bandwidths calculated from the impulse response shown in panel 1b (~500 kHz). This difference means our detector has different bandwidths for dynamic signal and noise. For the noise, a simplified noise analysis[18] of amplifiers with transimpedance design shows that the noise from op-amps is about 10 times the Johnson noise of R_f and arises primarily from the amplifier itself. The analysis gives an RMS noise of 0.62 mV and a noise bandwidth of 2.1 MHz for the gain setting G0, which match very well with the noise from the scope and the bandwidth from panel 1c, respectively. We have integrated the noise spectra in Figure 1c and obtained the RMS voltage noise on a 50 Ω load: 0.63, 0.84, 1.6, 2.6, 3.5, and 6.2 mV for G0, G1, G2, G4, G6, and G9 settings, respectively. They agree reasonably well with those measured by the scope. However, for shot noise, which is filtered as the photocurrent, the noise spectrum should be those measured by impulse response method shown in Figure 1b.

This bandwidth difference gives subtle difference of data correlation between detector noise and shot noise in the data processing of ring-down transients. Based on Figure 1b and c, if the data sample rate is 1 MHz (typical in our experiments) and no LP filters of narrower bandwidth is used after the detector, with eq 2, the detector noise can be treated as uncorrelated in LSF process, but the A/D recorded noise σ will contain extra noise from aliasing of frequency components above the Nyquist frequency 500 kHz in noise spectra. The limiting bandwidth of shot noise is about 500 kHz from Figure 1b, which gives a time scale of correlation about 0.3 μs. Below we will demonstrate that the effect of this shot noise correlation on the sensitivity of cw-CRDS is not important if the ring-down signal is near DNL situation.

The ring-down transients in our experiments are recorded by a four-channel 12-bit A/D converter (PCI-DAS4020/12, Measurement Computing). The typical sample rate used is 1 MHz. The input range of each channel is set to ±5 V, giving a bit size of 2.44 mV. As shown in Figure 1d, the 3 dB bandwidth of the A/D is measured to be 17 MHz by recording the RMS values of input sine waves of different frequencies but of constant amplitude. The bandwidth of the A/D is much larger than that of the detector. Its noise level is measured to be 1.45 mV, smaller than the bit size but comparable with the detector noise at lower gain settings.

To reduce the extra noise by aliasing in the sampling process, we have employed a LP "filter" between the output of the detector and the input of the A/D card, which consists of an RC LP filter followed by an amplifier containing a low-noise op-amp. The RC filter has a time constant of 0.656 μs, and the following amplifier has a continuously variable gain from 1 to 11. Shown in Figure 1e, the 3 dB bandwidth of this RC filter plus amplifier is measured to be 220 kHz by recording its response to an input sine wave with its frequency changing from 1 kHz to 2 MHz. The measured bandwidth is very close

dx.doi.org/10.1021/jp406691e | J. Phys. Chem. A XXXX, XXX, XXX−XXX

Table 1. Summary of the Analysis of 12 Ring-Down Data Sets[a]

data set no.	τ (μs)	δ_τ (μs)	σ_τ (μs)	rd rate (Hz)	σ_y (mV)	A (mV)	δ_A (mV)	$G8k\Delta t(\sigma_y/A)^2$, DNL	$(\delta_\tau/\tau)^2$, exp.	α_{min} (cm^{-1}/Hz$^{1/2}$)
1	220.99	0.058	0.038	4.2	2.32	3312	148	2.97×10^{-8}	6.89×10^{-8}	1.93×10^{-11}
2	220.99	0.059	0.038	4.0	2.32	3339	153	2.92×10^{-8}	7.13×10^{-8}	2.01×10^{-11}
3	220.99	0.056	0.038	5.1	2.32	3330	155	2.94×10^{-8}	6.42×10^{-8}	1.69×10^{-11}
4	221.11	0.057	0.038	2.8	2.35	3328	274	3.01×10^{-8}	6.65×10^{-8}	2.32×10^{-11}
5	223.43	0.072	0.038	9.6	2.35	3722	684	2.39×10^{-8}	1.04×10^{-7}	1.55×10^{-11}
6	223.49	0.080	0.037	9.8	2.35	3716	627	2.39×10^{-8}	1.28×10^{-7}	1.71×10^{-11}
7	223.70	0.073	0.038	7.8	2.35	3708	699	2.40×10^{-8}	1.06×10^{-7}	1.74×10^{-11}
8	222.88	0.066	0.025	31.2	1.53	4115	414	8.29×10^{-9}	8.77×10^{-8}	7.93×10^{-12}
9	222.87	0.088	0.025	6.1	1.53	4110	417	8.31×10^{-9}	1.56×10^{-7}	2.39×10^{-11}
10	221.01	0.059	0.040	3.1	2.30	3108	253	3.31×10^{-8}	7.13×10^{-8}	2.29×10^{-11}
11	221.07	0.067	0.039	3.6	2.32	3320	477	2.95×10^{-8}	9.19×10^{-8}	2.41×10^{-11}
12	221.05	0.065	0.038	2	2.34	3341	449	2.97×10^{-8}	8.65×10^{-8}	3.14×10^{-11}

[a]For each data set, τ is the ensemble average of the extracted decay time constants, and δ_τ is the corresponding standard deviation of extracted τ. σ_τ is used to denote the ensemble average of the predicted error of τ by each LSF. σ_y is explained in detail in the main text. A is the initial decay amplitude defined for t = 15 μs for a decay transient, and δ_A is the ensemble standard deviation of this fitted A for a data set. In this table, σ_τ, σ_y and A are ensemble average values. The square of the fractional noise of decay rate k, $(\sigma_k/k)^2$, is used to denote the noise level in k. G $8k\Delta t(\sigma_y/A)^2$ is the predicted $(\sigma_k/k)^2$ for DNL situation. With 220 kHz overall bandwidth, G = 1.67. $(\delta_\tau/\tau)^2$ is defined as the measured $(\sigma_k/k)^2$, which finally determines the true short-term sensitivity in our CRDS experiments. α_{min} is the sensitivity in cm^{-1}/(Hz$^{1/2}$) calculated with $(\delta_\tau/\tau)^2$ and the corresponding ring-down event rate. All of the data sets have a detector gain of 5 × 10^6 V/A except no. 8 and 9, for which the gain is 2 × 10^6 V/A. The antialiasing LP "filter" has a gain of 3.

to the calculated one of the RC filter, $1/(2\pi \times 0.656\ \mu s)$ = 243 kHz. Since the detector bandwidth (Figure 1b and c) is significantly larger than that of the RC LP filter, this 220 kHz will be regarded as the overall bandwidth of the combined detection system when it is used in experiments. This bandwidth gives G = 1.67 based on $G = \tanh^{-1}(k_f\Delta t/2)$,[8] with k_f the angular frequency of the 3 dB point. If the sample rate is 1 MHz, $k_f\Delta t$ = 1.38, close to the optimum value 1.[8]

In our experiments, the typical amplitude of ring-down transients at the output of the detector is about 1.3 V at detector gain 2 × 10^6 V/A (G1). The 12-bit A/D card has an input range of ±5 V. To fully utilize the input range of the A/D, at suitable gains (typically 3), the above "filter" can linearly transform the detector output signal to the A/D input range between −3 and 4 V, in which the A/D converter has excellent linearity. After the signal conditioning, the ring-down signal at the input of the A/D card will have a baseline B at −3 V (adjustable between −3 and 0 V). Each ring-down transient has 2000 data points corresponding to a recording time window of 2 ms. The first several data points after triggering are typically not used in the LSF because, first, they have excess noise and second, they can be distorted by detector saturation for very large signal. Furthermore, the highest voltage used in the LSF process, V_{max}, is set to 1 V at most of time or to 2 V for some experiments to avoid possible saturation. For very large ring-down transients, the first data point having voltage not larger than V_{max} is the starting point of the nonlinear LSF.

SENSITIVITY RESULTS WITH ANTIALIASING LP FILTER

Starting from this section, we will present results of sensitivity studies in our cw-CRDS experiments followed by discussions. Unlike our previous paper,[19] this article is focused on the sensitivity limits of CRDS method in a relatively short time period of several minutes.

The data presented in this section were recorded by our cw-CRDS setup using a distributed feedback (DFB) semiconductor laser of wavelength 1520 nm. At this wavelength the detector has a spectral response of 0.95 A/W and a quantum efficiency of 0.78. The ring-down cavity length is 39.5 cm, giving a free spectral range (FSR) of 380 MHz. We have realized a ring-down τ longer than 220 μs (mirror power loss of 6 ppm per reflection), the largest τ realized with the same cavity length in our lab. The cavity length is scanned by three PZTs attached to one cavity mirror to generate resonance between the laser and the ring-down cavity. The driving voltage is a triangle wave at 15 Hz with a scan range slightly more than one FSR of the cavity. The above-discussed antialiasing RC LP filter plus op-amp was inserted between the detector output and A/D input. In this way we have recorded multiple ensembles of ring-down decays for detailed analysis. Each ensemble contains several hundreds of decay transients captured within about 1 min and at a ring-down event rate from several Hz to tens of Hz. Each transient is fitted to eq 1 using the nonlinear LSF in which each data point of a transient is equally weighted, and the data correlation from filtering is ignored, as discussed in the model section. Even with the 4 mm diameter intracavity aperture,[16] several data sets still contain small size dropout of τ, typically with a dropping amplitude about 0.3 μs, which can be easily seen in a time series plot of τ. This kind of dropout is likely caused by the interference of high-order transverse modes which are resonantly excited when they are near degenerate with the TEM$_{00}$ mode in the cavity.[16] The data ensembles we have selected are those without τ dropouts and having a normal distribution of τ.

Table 1 summarizes the analysis results of 12 data sets and displays typical sensitivity realized by our cw-CRDS system. For the first four data sets, a semiconductor optical amplifier (SOA) is used as the light switch;[20] for the other eight ones, a conventional AOM is used. The extinction ratio of both switches have been measured to be higher than 75 dB.[9] For each ensemble, there are 11 quantities displayed. The definitions of these quantities are included in the caption of Table 1 except σ_y, which is explained in detail below. For a single decay transient, σ_y is defined as the standard deviation of the last 500 data points tail signal, which is also used to calculate the reduced χ^2 of each LSF. However, if amplitude A or/and τ is large enough, the last 500 data points tail will contain significant amount of decay information, making the

dx.doi.org/10.1021/jp406691e | J. Phys. Chem. A XXXX, XXX, XXX−XXX

Table 2. Shot Noise (SN) and Detector Noise Levels in Our CRDS Experiments[a]

data set no.	detector gain (V/A)	$G8k\Delta t(\sigma_y/A)^2$, DNL	$\xi^2k(h\nu/QA)$, SNL	$(\delta_\tau/\tau)^2$, exp.	A (μW)	SNPD (pW/(Hz$^{1/2}$))	SN (nW)	P_N (pW/(Hz$^{1/2}$))	σ_y (nW)
3	5×10^6	2.94×10^{-8}	9.69×10^{-9}	6.42×10^{-8}	0.234	0.281	0.165	0.277	0.163
5	5×10^6	2.39×10^{-8}	8.58×10^{-9}	1.04×10^{-7}	0.261	0.297	0.174	0.281	0.165
8	2×10^6	8.29×10^{-9}	3.12×10^{-9}	8.77×10^{-8}	0.722	0.493	0.290	0.457	0.268

[a]The detector transimpedance gain in column two does not include the gain 3 of the RC LP filter plus op-amp. $G8k\Delta t(\sigma_y/A)^2$ and $\xi^2kh\nu/QA$ are the predicted $(\sigma_k/k)^2$ for DNL and SNL cases, respectively, with $G = 1.67$ and $\xi^2 = 2.96$ (SN equally weighted). Also given in the table is the initial decay amplitude A in units of μW, followed by initial shot noise power density (SNPD), which is defined as $(2h\nu A/Q)^{1/2}$ in units of pW/(Hz$^{1/2}$). $P_N = (4\sigma_y^2/k_f)^{1/2}$ is the effective NEP of the detection system: detector, RC LP filter plus amplifier, and A/D converter. Both SNPD and P_N are defined for one-sided spectra. The initial shot noise power is calculated by $(k_f h\nu A/2Q)^{1/2}$ with $k_f = 2\pi \times 220$ kHz. σ_y is in units of nW.

calculated σ_y larger than its true value. Correspondingly the calculated reduced χ^2 will be substantially smaller than 1 (the value for a good fit). Therefore, with known A and τ, a correction excluding the residual decay signal in the tail has been made to obtain the correct noise level σ_y in Table 1. For example, without this correction, the ensemble reduced χ^2 is about 0.66 for the data sets with A about 4.1 V in Table 1. After this correction, all of the reduced χ^2 is close to 1 (not shown in Table 1).

From Table 1, we can draw the following conclusions:

- Ring-down time constant τ changes from one experiment to another. This is likely from the system drift caused by changes in the lab environment.[19]
- δ_τ, the observed ensemble standard deviation of τ, is always larger than $(G)^{1/2}\sigma_\tau$, the predicted error of τ by single LSF including data correlation.[8] Correspondingly, the predicted DNL $(\sigma_k/k)^2$ with G correction factor, is always less than the measured one $(\delta_\tau/\tau)^2$.
- Data set no. 8 shows that a higher ring-down event rate will increase the short-term sensitivity of CRDS experiments substantially.[15] This higher ring-down event rate was achieved by keeping the resonance between the laser and the cavity TEM_{00} mode through manually adjusting the PZT voltage to control the cavity length. Since completing these measurements, we have implemented a locking scheme where a small modulation of the cavity is used (~ 20 MHz peak-to-peak) and the modulation voltage when the ring-down event is triggered is used to adjust the DC level on the PZTs. This increases the ring-down event rate by up to an order of magnitude and also reduces the number of decays that result from triggering on higher order modes (which have resonances outside of the modulation interval).
- The four data sets No. 1–4 using SOA as the light modulator have smaller $(\delta_\tau/\tau)^2$ than those using an AOM and have δ_A several times smaller than those of AOM.

In the experiments, we have observed about 29% decrease of the predicted σ_τ when the antialiasing LP filter was added between the detector and A/D input with the same trigger threshold setting. This decrease is a direct result of both the detection bandwidth reduction from data filtering and ignoring data correlation in the LSF. σ_τ reflects the effect of the short-term noise in the detector voltage and does not reflect changes in τ from other effects, such as slow environmental changes in temperature or barometric pressure. Because the mirrors have a strong spatial dependence in their loss, a change in the position of the TEM_{00} mode on the mirrors a small fraction of the mode size can cause shifts in τ far higher than the short-term noise. In Table 1, $(G)^{1/2}\sigma_\tau$, the correct error estimation of τ by LSF, is always less than δ_τ for all data sets. This is because, besides detector noise and shot noise, δ_τ (standard deviation of τ of a data set) typically contains contribution of broader noise sources, for example, fluctuation of amplitude A (see below). Only when the CRDS system is completely limited by shot noise and stable detector noise, with constant A shot to shot and measurements occur over an time interval for which cavity drift is negligible, will $(G)^{1/2}\sigma_\tau$ be equal to δ_τ. In our measurements, the predicted $(\sigma_k/k)^2$ (with G factor) in Table 1 is about several times less than the measured one $(\delta_\tau/\tau)^2$.

We believe the conclusion in the last bullet is due to the fact that an SOA has a faster turning off speed than an AOM. An SOA can turn off the incident light within several nanoseconds upon triggering,[20] compared with 1 μs order speed by an AOM. With slower turning off speed of an AOM, the intracavity optical field takes longer time to start its exponential decay, which leads to the fact that the randomness of the initial decay amplitude A (defined at $t = 15$ μs) when using an AOM is larger than that when using an SOA. While the nonlinear relationship of k to the data means that the LSF introduces bias that scales as $(\sigma/A)^2$,[8] this is far below the fluctuations in k from the noise (which scale as (σ/A)). The increase of δ_τ by larger δ_A is too small to explain the observed noise correlations of A with k in Table 1. We attribute these correlations to the effects of possible small nonlinearities in our detection electronics. The advantages of using faster light switch such as an SOA in cw-CRDS are, first, that it gives smaller randomness in initial decay amplitude A and hence can improve final sensitivity; second, the time window skipped for LSF is shorter if the decay signal is not saturated by any other factors.

Table 2 gives shot noise and detector noise levels in our experiments. Three typical data sets are selected from Table 1. From Table 2, we can see that the initial shot noise level is close to the detector noise level. Correspondingly, the predicted $(\sigma_k/k)^2$ of SNL cases is about 8 times less than that of DNL. Table 2 has listed both predicted sensitivity limits of DNL and SNL cases, plus the measured one $(\delta_\tau/\tau)^2$. We could not find closed form expressions for the sums of the curvature matrix (and thus the predicted statistical noise in k) when both shot and detector noise contribute. As an approximation, we can use the sum of both limits as an estimation of the overall sensitivity limit. We found the sum is several times less than the observed one in our CRDS experiments (see further discussion in next section). Including both noise sources, the initial signal-to-noise ratio (S/N) of our decay transients in Table 1 is slightly less than 1000.

EFFECTS OF SHOT NOISE ON REDUCED χ^2 AND SENSITIVITY

The reduced χ^2 in previous sections assumes each data point in a decay signal has the same noise level. However, as displayed in Table 2, our ring-down transients contain both detector noise and comparable initial shot noise, which decays at a rate of $k/2$. One direct result of this decaying shot noise is that the

dx.doi.org/10.1021/jp406691e | J. Phys. Chem. A XXXX, XXX, XXX–XXX

ensemble average of the above reduced χ^2 for all the data sets in Table 1 is slightly larger than 1, ~1.1 (except 0.98 for data set no. 4). This is because the sum of squares of fitted residuals, which contain both shot noise and detector noise contribution, is scaled to detector noise σ_y^2 only. With shot noise, the correct reduced χ^2 should include different weights for each data point of a decay transient:

$$\chi^2_{\text{red}} = \frac{1}{\kappa}\sum_{i=0}^{N-1} w_i(y_i - Ae^{-kt} - B)^2 \tag{11}$$

$w_i = \langle \varepsilon(t_i)^2\rangle^{-1}$ (see eq 2 and 3) is the weight for i^{th} data point. Its ensemble average is $\langle\chi^2_{\text{red}}\rangle$. We use $\langle\rho^2_{\text{red}}\rangle$ to denote the ensemble average of previous (detector noise weighted) reduced sum of squares of fitted residuals for each data set,

$$\langle\rho^2_{\text{red}}\rangle = \frac{1}{\kappa\sigma_y^2}\sum_{i=0}^{N-1}\langle y_i - Ae^{-kt} - B\rangle^2 \tag{12}$$

In fact, if we assume shot noise and detector noise are not correlated with each other, under conditions of $N\Delta t \gg \tau$ and $\Delta t \ll \tau$, the above equation reduces to

$$\langle\rho^2_{\text{red}}\rangle = 1 + \frac{\tau}{\kappa\Delta t}\frac{2h\nu A}{QP_N{}^2}\frac{k_{Sf}}{k_{Df}} \tag{13}$$

In the above three equations, y_i are the data points, N is the total number of data points used in LSF, τ is the decay time constant, κ is the number of degrees of freedom in LSF, Δt is the inverse of the A/D digitization rate, h is Planck constant, ν is the laser frequency, A is the initial decay amplitude (first data point of LSF) in units of watt, Q is the quantum yield of the detector, P_N is the NEP of the detection system, and k_{Sf} and k_{Df} are the limiting bandwidths of shot noise and detector noise, respectively. As shown in Figure 1b and c, they can be different if there is no LP filter of smaller bandwidth used after the detector. In eq 13, the first term is from the detector noise, and the second term is the contribution from shot noise, which linearly depends on the amplitude A.

To explore subtle effects of shot noise in CRDS experiments, we have recorded 1376 ring-down decay transients continuously in 2 min at a sample rate 1 MHz. The laser wavelength is 1652 nm. The detector gain was set to 5×10^6 V/A. For shot noise, the 3 dB bandwidth is 420 kHz (Figure 1b), and for detector noise, it is about 3 MHz (Figure 1c). At this wavelength, the detector has a spectral response of 0.85 A/W and a quantum efficiency of 0.64. The cavity length was modulated at 12 Hz by three PZTs with a scan range slightly larger than one FSR. An AOM was used to switch the incident laser off when the detector signal reached the 1.2 V trigger threshold. Upon triggering, the intracavity light field fluctuates substantially near the threshold voltage during the first ~5 μs before the intracavity light intensity starts to decay exponentially. After LSF data processing (eqs 4 and 5), we found the ensemble average of fitted A (here defined for time zero) is 1355 mV, with standard deviation 327 mV. This means that, even with the same trigger threshold, the initial amplitude A fluctuates significantly from shot to shot when the cavity is excited by a noisy laser.

This ensemble of 1376 ring-down transients is first processed by three-parameter LSF then by two-parameter LSF, with different initial decay amplitudes ranging from 400 mV to 2000 mV, with a step of 100 mV. The details of this data analysis will be given below. The purpose of this is to demonstrate how different shot noise levels, that is, different sizes of A, affect the sensitivity of CRDS experiments. To fully avoid the noisy beginning part of ring-down signal, the first seven data points are skipped in LSF. For each amplitude A, only the transients with signal level at 7 μs (eighth data point) not less than A are selected and fitted to eq 1, while those transients with the signal at 7 μs less than the preset amplitude are ignored. Therefore, for each preset amplitude, not all of the 1376 transients are selected because of the randomness in A. For examples, there are 1376 decays selected for amplitude 400 mV, 843 decays for 1200 mV, and only 34 decays for 2000 mV. The LSF starts at the first data point at which the signal is not larger than the preset A, and the data points with signal larger than A are skipped. Thus, the total number of data points used in LSF for each transient is less than 2000. To keep the number of degrees of freedom κ constant for those selected transients, we have elongated those truncated transients back to 2000 data points in total by adding more data points to the tails. For each of such transients, the added data points are pseudo random numbers generated by using the mean and standard deviation of the tail (last 500 data points) of the transient, which contain negligible residual decay information for this data set.

Different from eqs 4 and 5, we have performed weighted LSF by numerical calculations to the 1376 ring-down transients. The weight matrix W is diagonal, and its i^{th} diagonal element is

$$w_i = \frac{1}{\sigma_y^2 + (k_{Sf}/2)(h\nu/Q)Ae^{-ki\Delta t}} \tag{14}$$

All of the parameters in this equation have been defined before, and k_{Sf} is the limiting bandwidth (angular frequency) of shot noise. Based on the discussion before, although the detector noise can be treated as uncorrelated in LSF because of a bandwidth of 2−3 MHz, this diagonal weight matrix W means we have ignored the shot noise correlation caused by a bandwidth of 420 kHz of G2 setting. Our previous study[8] shows that the bias error of extracted decay rate k caused by ignoring data correlation in this nonlinear LSF is negligible when compared with the final σ_k which includes the contribution of all kinds of noise. In fact, as demonstrated in this section, if ring-down transients are mainly detector noise limited, as in our experiments, including shot noise correlation in the weight matrix by numerical calculations only produces negligible correction to both k and σ_k (ensemble standard deviation of fitted k). Furthermore, the correction to extracted k when switching from equally weighted LSF (eqs 4 and 5) to one with a diagonal weight matrix including both shot noise and detector noise (eq 14) is also negligible if the data are DNL.

With the diagonal weight matrix defined by eq 14, for each preset A, we have numerically calculated $\langle\rho^2_{\text{red}}\rangle$, $\langle\chi^2_{\text{red}}\rangle$, and the standard deviation of extracted decay rate k for both three-parameter LSF and two-parameter LSF. For each decay transient, an equally weighted three-parameter LSF (eqs 4 and 5) is performed first to obtain an estimation of initial decay amplitude A, which is then used to calculate the shot noise of each data point in the second weighted LSF. The detector noise σ_y in eq 14 is calculated to be 2.357 mV (equivalent to 5.55×10^{-10} W at 1652 nm) from all 1376 ring-down tails (last 500 data points) after the subtraction of tiny residual decay amplitude. This detector noise should contain the contribution by aliasing in the under sampling process of the noise with 1 MHz sample rate. Assuming we have a stable baseline during

dx.doi.org/10.1021/jp406691e | J. Phys. Chem. A XXXX, XXX, XXX−XXX

this 2 min time period, this σ_y has an accuracy of $1/(1376 \times 500)^{1/2} \approx 0.1\%$. As shown below, this accuracy is very important in obtaining the linear dependence of A in eq 13.

Figure 2 is a plot of $\langle\rho^2_{red}\rangle$ versus initial decay amplitude A (in μW), showing a clear linear relationship. It is generated by the

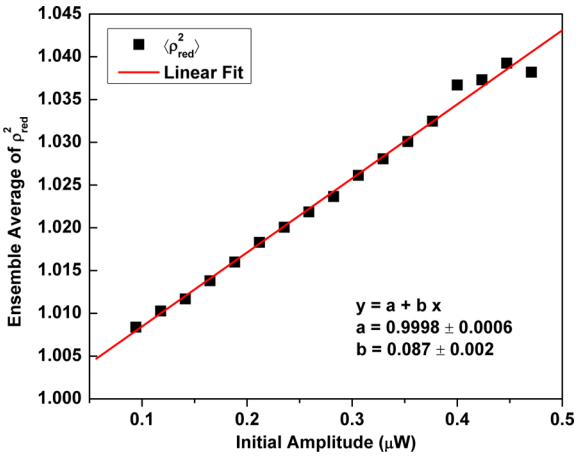

Figure 2. $\langle\rho^2_{red}\rangle$ versus initial decay amplitude A, calculated with k_{Sf} = 1.338 × 2π × 420 kHz. Data points of larger A become noisy because of the smaller ensemble size for larger A.

weighted three-parameter LSF, but no noticeable difference is observed for the one by weighted two-parameter LSF. Each point in the plot is an ensemble average of ρ^2_{red} of the selected transients for a preset A. With σ_y = 2.357 mV fixed and only adjusting the bandwidth k_{Sf}, surprisingly, we found when k_{Sf} = 1.338 × 2π × 420 kHz = 3.531 × 10^6 rad/s, the $\langle\chi^2_{red}\rangle$ is very close to 1, between 0.998 and 1.001 for all of the amplitudes. This is true for both two-parameter and three-parameter weighted LSF. When performing two-parameter LSF, a fixed baseline of −4.400 mV was used, which is also an average of all 1376 tails. In eq 14, k_{Sf} is directly related to the shot noise power of each data point. The above result shows that, in order to best describe the total "shot noise" in our CRDS signal, the effective bandwidth of shot noise is 1.338 times of the one measured by the impulse response method, which further implies the existence of shot noise like extra noises in the signal. In the data analysis in this section, we will use this effective k_{Sf} as the bandwidth of shot noise. This optimization of k_{Sf} causes negligible change in extracted k.

In Figure 2 the slope of the linear dependence in Figure 2 is 87 000 W^{-1}, with a near unity intersect of 0.9998. For the highest A 0.47 μW (equivalent to 2 V signal), the $\langle\rho^2_{red}\rangle$ is only 4% higher than 1, meaning the contribution from the shot noise is relatively small for our data. Thus a less accurate σ_y will deteriorate the linear plot greatly. The 1376 decays have an averaged τ of (169.06 ± 0.11) μs. With the above slope and putting all of the known parameters into eq 13, we have calculated the NEP of the detection system at gain 5 × 10^6 V/A of G2 to be P_N = 2.62 × 10^{-13} W/(Hz$^{1/2}$). In another way, with k_{Df} = 2π × 3 MHz and σ_y = 2.357 mV, the detector NEP is P_N = $2\sigma_y/(k_f^{1/2})$= 2.55 × 10^{-13} W/(Hz$^{1/2}$), very close to the above one. Converted from the electrical noise power spectral density in Figure 1c, the detector NEP at G2 setting is calculated to be 2.35 × 10^{-13} W/(Hz$^{1/2}$) at 1652 nm, which is slightly smaller than the above two values, possibly caused by using a quieter power supply in Figure 1c. The above NEPs are on the same order of those in Table 2.

One may try to explain the linear trend in Figure 2 by the nonlinearity of the detector output or the A/D card. Our A/D card has an input range of ±5 V and 12-bit resolution. In the range of 0−4 V, the single linear sweep from an Agilent function generator was recorded by the A/D, and a linear fit to it gives an RMS noise of 1.33 mV for each data point, which is close to the measured A/D noise of 1.45 mV. With a bit size of 2.44 mV, the RMS noise means that between 0 and 4 V, the probability for each voltage step of the A/D card to have one bit reading error is only about 5%. On the other hand, if the largest $\langle\rho^2_{red}\rangle$ = 1.038 of 0.47 μW (equal to 2.0 V) is caused by systematic reading error of A/D, then the A/D reading error at 2.0 V will be about one bit size 2.44 mV, which is inconsistent with the above analysis. More importantly, the systematic error of A/D would make $\langle\rho^2_{red}\rangle$ proportional to A^2, not A. This argument is also true for the possible nonlinearity from the detector.

Figure 3 plots the variance, square of the ensemble standard deviation, of extracted decay rate k, σ_k^2, versus initial decay

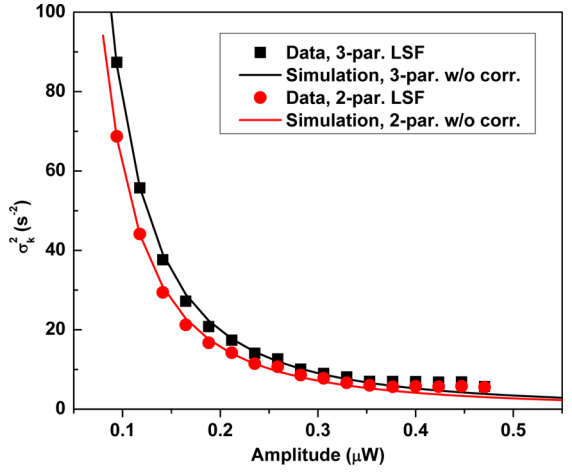

Figure 3. Square of ensemble standard deviation of fitted decay rate k, σ_k^2, versus initial decay amplitude A. The data points are from three-parameter or two-parameter weighted LSF, and the two corresponding best fit curves are the predicted variances of k by the covariance matrix.[8] Both the weighted LSF and the covariance matrix do not contain shot noise correlation caused by limited detector bandwidth.

amplitude A. As expected, σ_k^2 decreases quickly with the increase of S/N. The square data points are from three-parameter weighted LSF and the circles from two-parameter weighted LSF, which are significantly lower than the squares for small amplitudes. This decrease of variance in two-parameter LSF is the result of the removal of strong correlation between k and baseline B when B is fixed to −4.400 mV. For large A and with N = 2000, the decay signal extends to the tail, and the difference between two methods is much smaller. Two corresponding curves are the best fits to the data points in the plot. They were generated by using the covariance matrices which do not contain shot noise correlation, that is, using a diagonal weight matrix. The covariance matrices used are similar to those of eqs 6 and 7 but with the weight matrix of eq 14. With k_{Sf} = 1.338 × 2π × 420 kHz, the best fits are achieved with 1.083σ_y for three-parameter covariance matrix and 1.076σ_y for two-parameter one. If the shot noise correlation is included in W, best fits are reached with 1.080σ_y for the three-parameter case and 1.076σ_y for the two-parameter one. The small change in detector noise of best fits is caused by shot noise data

dx.doi.org/10.1021/jp406691e | J. Phys. Chem. A XXXX, XXX, XXX−XXX

correlation.[8] This confirms that the effect of shot noise correlation on σ_k^2 is small for our data. The detector noise of both best fits are about 8% higher than σ_y. We believe this is caused by extra noises in our system, for example, the data points in the plot plateau at large A while both predictions keep decreasing, which can be caused by small nonlinearities in our detection system for large signal.

Figure 4 is a log−log plot version of Figure 3 with A extended to broader range, reaching both DNL and SNL

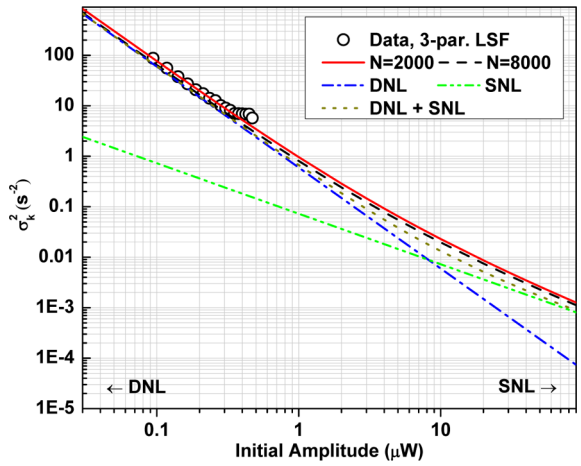

Figure 4. σ_k^2 versus initial decay amplitude A. The data points are from three-parameter weighted LSF without including shot noise correlation. The solid curve is the error prediction of k from the three-parameter covariance matrix with N = 2000, and the dashed line is the same prediction with N = 8000, both without including data correlation; that is, a diagonal weight matrix was used. The dash-dot-dashed line is the theoretical limit of DNL situation (eq 8), and the dash-dot-dot-dashed line is the one of SNL case with correlation (eq 10). The dotted line is the direct sum of DNL and SNL predictions. The plot clearly shows that the 1376 CRDS transients are near the DNL side.

situations. The plot also includes predicted variances of k under different assumptions. In Figure 4, the data points are from three-parameter LSF with the diagonal weight matrix eq 14. It is clear that our CRDS experiments are more DNL and the measured variance of k plateaus at larger A more clearly in this log−log plot. The solid line is σ_k^2 from the three-parameter covariance matrix with N = 2000 and a diagonal weight matrix. It reaches the best fit with $1.083\sigma_y$, which is slightly larger than $1.080\sigma_y$ of the best fit with three-parameter covariance matrix including shot noise correlation (not shown for clarity), which is almost the same as the solid line near the DNL side but starts to deviate from the solid line with A increasing. At A = 90 μW, it is only 4.5% less than the solid line. In the simulation, the weight matrix with shot noise correlation is generated by numerically calculating the inverse of the sum matrix between the diagonal detector noise covariance matrix and the one of correlated shot noise (eq 2). The dashed line is the prediction with a diagonal weight matrix (eq 14) but with N = 8000, which is about 13−20% less than the solid line. Previously we have proved that, in three-parameter LSF, the predicted variance of k reaches the theoretical limit of $N = \infty$ much slower than in two-parameter LSF because of the correlation between k and B.[8] The difference between the solid line and the dashed line is the direct result of this correlation. The dash-dot-dashed line is the theoretical limit of k variance of DNL situation from eq 8 with $\sigma = 1.083\sigma_y$, and the dash-dot-dot-dashed line is the one of SNL but with correlation, that is, eq 10, and ξ^2 = 1.87 (k_{Sf} = 3.531 × 10^6 rad/s). Near the DNL side, the DNL variance is much larger than the SNL one and vice versa near the SNL side. The dotted line is the sum of DNL and SNL predictions. When both detector and shot noise are included in the fitting model, there is no analytical formula of the k variance available from a single decay transient as for the DNL or SNL case. One may use the direct sum of DNL and SNL predictions to estimate the variance of k. As can be seen from Figure 4, the sum is always less than the true value of the N = 8000 line, which reflects that a longer fit interval of the three-parameter LSF will produce a lower variance of the fit parameters. The direct sum works well (only about 5% below the N = 8000 line) near the DNL side but can be 50% less than the N = 8000 line for large amplitudes near the SNL side.

The other similar log−log plot (not shown here) is of two-parameter simulation with B fixed to −4.4 mV. With the removal of the correlation between k and B, the predicted variance of k is significantly smaller than that from three-parameter case, as displayed by Figure 3, and the N = 2000 line and the N = 8000 line from two-parameter covariance matrix almost overlap with each other.

The last comment on this data set of 1376 transients is about data correlation. With $k_{Df} = 2\pi \times 3$ MHz and k_{Sf} = 3.531 × 10^6 rad/s, the data correlation time scales of detector noise and shot noise are the inverse of them, that is, 0.05 and 0.3 μs, respectively. Both are less than the sampling interval 1 μs and hence suggest that the data correlation in the signal should be small. We have calculated the averaged autocorrelation of the 1376 fitted residual traces. For this purpose, the equally weighted LSF version is used, with no data correlation included, and the first seven data points skipped for each transient. The ensemble averaged autocorrelation is almost a Dirac δ-function at zero time delay, having a peak value of 5.79 mV^2, which is larger than σ_y^2 = 5.56 mV^2 because of the contribution from shot noise. At 1 μs time delay, the correlation is about 2% of the peak value and decays to zero near 400 μs time delay. This long tail likely arises from the excess low frequency noise of the system.

OPTIMIZATION OF SENSITIVITY OF CW-CRDS

If we observe M ring-down events per second and we assume that their noise is uncorrelated (which should be the case if we truly are detector or shot noise limited (or both)), then we expect the noise per root Hertz to be $\sigma_k/(M)^{1/2}$. What is the optimal values to set the trigger power and the length of time we should fit? Larger I_{th} and N decrease the value of σ_k but also decrease the rate at which transients are detected. We will now present the results of such an optimization.

If the exciting laser is left on resonance with the cavity (with a frequency shift small compared to the combined width of the laser and cavity) for long compared to a cavity lifetime, the mean transmitted power of an empty cavity will be given by[9,21,22] $I_0 = (T/(1-R))^2(1 + 2\pi\Delta\nu_L\tau)^{-1}I_L$, where T and R are the power transmission and reflectivity of the mirrors that make up the CRDS cavity (assumed to be identical), $\Delta\nu_L$ is the FWHM of the laser frequency spectrum (assumed to have a Lorentzian line shape), and I_L is the optical power of the laser imaged onto the TEM_{00} mode of the cavity. In most practical CRDS experiments, $\Delta\nu_L\tau \gg 1$, or equivalently, the decoherence rate for the laser $D = \pi\Delta\nu_L \gg k$. In this case, the mean transmission of light on the detector is $I_0 = (T/(1 -$

dx.doi.org/10.1021/jp406691e | J. Phys. Chem. A XXXX, XXX, XXX−XXX

$R))^2(k/2D)I_L$. The effect of an intracavity absorber can be included by replacing T with $T\exp(-\alpha L/2)$ and R with $R\exp(-\alpha L)$ where α is the sample absorption coefficient and L is the length of the sample between the mirrors. However, there is considerable noise in this transmitted intensity since the light fields entering the cavity at times separated by more than $1/D$ are uncorrelated and thus add with a random relative phase. As previously discussed,[8,21] this leads to a χ^2 with two degrees of freedom distribution (for the in and out of phase components of the light field), $P(I) = \exp(-I/I_0)/I_0$. $P(I)$ is the probability density when the transmitted light power is I. If the light is suddenly allowed to excite an empty cavity at $t = 0$ with its central frequency matching a cavity resonance, then for $t \gg D^{-1}$, the mean light intensity on the detector will follow $\langle I(t)\rangle = I_0(1 - \exp(-kt))$, and again with a χ^2 with two degrees of freedom distribution fluctuations around that mean.

The equation $P(I) = \exp(-I/I_0)/I_0$ implies that the logarithm of triggering frequency has a linear dependence with the threshold I_{th} and the slope of the straight line is $-1/I_0$. Therefore this equation can be used to measure I_0. In real experiments, if the laser frequency is not locked to the TEM_{00} mode of the cavity, it is difficult to keep the incident laser on resonant with the cavity mode for a long time because of laser frequency instability. Here we have tried an easy way to observe this linear behavior. In the measurement, the laser frequency was fixed, and the cavity length, hence the resonance frequency of the TEM_{00} mode, was modulated through three PZTs attached to one cavity mirror mount. The ramp signal is 15 Hz triangle wave with a modulation range slightly more than one FSR of the cavity, which is about 380 MHz. The relative frequency sweeping rate is 11.4 GHz/s. The diode laser used has a short-term linewidth of 1 MHz.[9] Therefore the excitation time of the cavity during each sweep is about 90 μs, significantly less than one $\tau \approx 220$ μs. In this measurement, we have counted the trigger times in 2 min for a series of trigger thresholds and plotted the natural logarithm of the trigger times versus the trigger threshold I_{th}. Unlike in typical cw-CRDS experiments, the laser was not turned off when the cavity output intensity reached the threshold. Upon each trigger event, there exists 3 ms dead time of the trigger box to prevent multiple triggering in a single sweep. The resonant point during each sweep (half cycle of the triangle wave) is always near the center of the sweep. The antialiasing filter was not used when this data was acquired.

Even with this relatively short excitation time, the linear behavior discussed above still exists, as displayed in Figure 5. With the triggering point near the center of each sweep, the maximum possible triggering times in 2 min is 3600 if only one trigger happens in each sweep, which is much larger than the highest trigger times recorded, 1086 times for the threshold 0.7 V. From the linear fit, the absolute value of the inverse of the slope is 1.28 V at detector gain of 5×10^6 V/A, or 0.51 V at detector gain of 2×10^6 V/A. Based on previous discussion in this section, the averaged peak transmission through the cavity is estimated to be $1 - \exp(-90/220) = 0.336$ of I_0. On the other hand, our previous detailed studies show that the same peak transmission is about 34% of I_0 if the relative scan rate is 11.4 GHz for our system.[9,22] Both results agree very well. Therefore we estimate I_0 to be 1.5 V for detector gain 2×10^6 V/A in our experiments.

We have numerically simulated a large number of cavity "build-ups" from a cold cavity treating the laser phase undergoing a random walk which is a good model for a

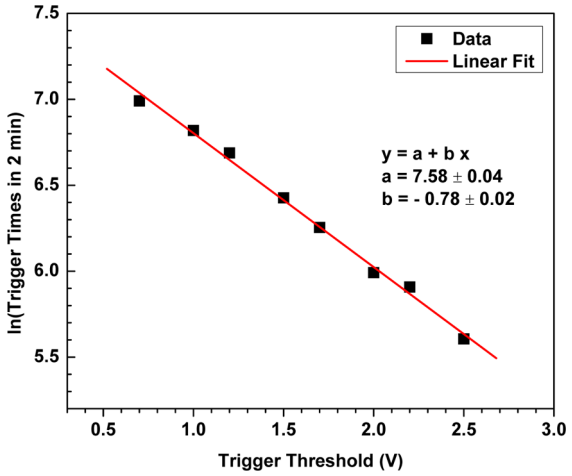

Figure 5. Plot of the natural logarithm of the trigger times in two minutes versus trigger threshold. The equation displayed is the linear fitting of the data. If there is no relative frequency scan between the laser and TEM_{00} mode, the absolute value of the inverse of its slope gives I_0. With a relative scanning rate of 11.4 GHz/s, this fitted value is about 34% of I_0.[9] The detector gain is 5×10^6 V/A.

diode laser.[22,23] It is found that the mean time before the detector light intensity reaches the trigger threshold I_{th} is given by $\langle \Delta t_{trig}\rangle = 0.861\tau \exp(0.787I_{th}/I_0)$ for $I_{th} > 1.0I_0$, independent of D as long as $Dt \gg 1$. If we observe the cavity decay for a time $N\Delta t$, the average rate that cavity decays will be observed is $(\langle \Delta t_{trig}\rangle + N\Delta t)^{-1}$. We assume that the laser can be switched on and the cavity begins being re-energized immediately after the end of the fitting time interval. For the DNL case, we have found that the values of $I_{th} = 3.96I_0$ and $N\Delta t = 10.8\tau$ give the lowest standard error in k (which gives $\langle \Delta t_{trig}\rangle = 19.4\tau$), for a net rate of ring-down events 0.033 k. These parameters give a noise per root Hz of k equals $3.14k(P_N/I_0)$. This result is summarized in the first row of Table 3.

To show how low the final detection limit can be in a short integration time period ($\sim$ 1 min), we plug numbers from our experiments into the above formula. We will take ensemble No. 8 in Table 1 as an example, which has the highest ring-down event rate of 31.2 Hz in all data sets. For this data the cavity length was not scanned. Its high ring-down event rate was realized by manually tuning the cavity length to the resonance through carefully adjusting the PZT control voltage. Data No. 8 has the lowest detection limit in Table 1 with $\alpha_{min} = 7.93 \times 10^{-12}$ cm^{-1}/(Hz$^{1/2}$). In this calculation, $\tau = 222.88$ μs, and I_0 is $1.5 \times 3 = 4.5$ V or 0.788 μW (the total gain is 6×10^6 V/A). The NEP of the combined detection system, that is, detector, antialiasing filter and A/D converter, is measured to be $P_N = 4.57 \times 10^{-13}$ W/(Hz$^{1/2}$). The optimum detection limit is $\alpha_{min} = 3.14kP_N/cI_0 = 2.7 \times 10^{-13}$ cm^{-1}/(Hz$^{1/2}$) with c the speed of light. Thus the measured sensitivity is about 29 times lower than the optimized DNL one. The optimum trigger threshold $3.96I_0 = 17.8$ V, which is about 4.3 times larger than the real threshold and cannot be realized with our setup due to the limitation of amplifier and A/D digitizer. The optimum threshold implies an S/N about 11 600 for our cw-CRDS system if the signal is only DNL. In fact, for such a high amplitude, the initial shot noise power is larger than the detector noise of our system. Including shot noise, the initial S/N is reduced to about 5600. Moreover the realized ring-down event rate 31.2 Hz is only about 1/5 of the optimum one

dx.doi.org/10.1021/jp406691e | J. Phys. Chem. A XXXX, XXX, XXX−XXX

Table 3. Optimum Sensitivities of cw-CRDS under Different Noise and Excitation Conditions[a]

Conditions	LSF par.	I_{th}	$\langle\Delta t_{trig}\rangle$	$N\Delta t$	rd rate	σ_k	σ_k
DNL, $\Delta\nu_L \gg \Delta\nu_c$	A,k,B	$3.96I_0$	19.4τ	10.8τ	$0.033k$	$3.14k(P_N/I_0)$	$3.14 \times 2D((1\text{-}R)/T)^2(P_N/I_L)$
DNL, $\Delta\nu_L \gg \Delta\nu_c$	A,k	$3.31I_0$	11.7τ	3.53τ	$0.066k$	$2.40k(P_N/I_0)$	$2.40 \times 2D((1\text{-}R)/T)^2(P_N/I_L)$
DNL, $\Delta\nu_L \approx \Delta\nu_c$	A,k	$1.21I_0$	7.28τ	3.27τ	$0.095k$	$5.52k(P_N/I_0)$	$5.52(k + 2D)((1\text{-}R)/T)^2(P_N/I_L)$
DNL, $\Delta\nu_L \ll \Delta\nu_c$	A,k	$0.898I_0$	5.90τ	3.16τ	$0.11k$	$6.93k(P_N/I_0)$	$6.93k((1\text{-}R)/T)^2(P_N/I_L)$
SNL, $\Delta\nu_L \gg \Delta\nu_c$	A,k	$2.47I_0$	6.01τ	5.67τ	$0.086k$	$2.31k(h\nu/QI_0)^{1/2}$	$2.31(2Dk)^{1/2}((1\text{-}R)/T)(h\nu/QI_L)^{1/2}$
SNL, $\Delta\nu_L \approx \Delta\nu_c$	A,k	$1.04I_0$	5.00τ	5.51τ	$0.095k$	$3.40k(h\nu/QI_0)^{1/2}$	$3.40((k + 2D)k)^{1/2}((1\text{-}R)/T)(h\nu/QI_L)^{1/2}$
SNL, $\Delta\nu_L \ll \Delta\nu_c$	A,k	$0.831I_0$	4.86τ	5.49τ	$0.097k$	$3.77k(h\nu/QI_0)^{1/2}$	$3.77k((1\text{-}R)/T)(h\nu/QI_L)^{1/2}$

[a]With the cavity TEM_{00} mode FWHM $\Delta\nu_c = 1/2\pi\tau$, the cavity mean transmission $I_0 = (T/(1-R))^2(1 + 2\pi\Delta\nu_L\tau)^{-1}I_L$ will be $(T/(1-R))^2I_Lk/2D$ if $\Delta\nu_L \gg \Delta\nu_c$, and $(T/(1-R))^2I_L$ if $\Delta\nu_L \ll \Delta\nu_c$, with $D = \pi\Delta\nu_L$. See main text for the definitions of all quantities. In the last column, the sensitivity σ_k has been converted into the form which only contains the parameters of a CRDS system. "5.90τ" in the fourth row and "4.86τ" in the last row are the built-up time before triggering when $\Delta\nu_L \ll \Delta\nu_c$. Note that the ring-down decay rate $k = c(1-R)/L$ depends on both mirror reflectivity R and cavity length L, with c the speed of light.

$0.033k$ = 148 Hz, limited by the extra laser frequency instability at acoustical frequencies.[9]

If the detector/amplifier is sufficiently stable, one can treat the baseline parameter, B, as fixed in the LSF. This reduces the noise in k for finite length fits to the decay due to correlations of the k and B. The curvature matrix is the same as above but with the row and column for B removed. Optimization with the two fit parameter covariance matrix gives values $I_{th} = 3.31I_0$ (which gives $\langle\Delta t_{trig}\rangle = 11.7\tau$) and $N\Delta t = 3.53\tau$ for a net rate of ring-down events of $0.066\ k$. These give a noise per root Hz of k equals $2.40k(P_N/I_0)$, a modest improvement by fixing B, and the result is summarized in the second row of Table 3. In order to correct for slow drifts in B, we have exploited a strategy where the data are fit both with fixed and variable B values. Sample absorbance is calculated by averaging k values computed from fixed B fits, but the assumed B value is slowly updated by averaging the B values determined from variable B value fits.

Recalling that I_0 is proportional to k if the laser linewidth $\Delta\nu_L$ is much larger than the cavity mode width $\Delta\nu_c$, we have the counterintuitive result that the sensitivity limit is independent of k, for example, changing k by adjusting cavity length L but with the reflectivity of mirrors fixed. (See the first and second line of the last column of Table 3.) This will fail when k is no longer much smaller than D, and σ_k will start to increase as $k \rightarrow D$ either by shortening L or decreasing mirror reflectivity R. The third row of Table 3 is the result of $\Delta\nu_c \approx \Delta\nu_L$, or $k \approx D$. For $k \gg D$, the detector power will saturate at $(T/(1-R))^2I_L$. The fourth row of Table 3 is for this case, that is, DNL signal but $\Delta\nu_L \ll \Delta\nu_c$. In this case the intracavity light field builds up exponentially with time before triggering. (See below for more details.) The sensitivity has an overall k dependence. Furthermore, we have neglected shot-noise in the detected signal, which will dominate over the detector noise for sufficiently large detector signal, $I_{th} \gg P_N^2Q/2h\nu$ where Q is the detector quantum efficiency.

The case of SNL CRDS has been previously considered.[7,8] For the two-parameter fit, the curvature matrix is the same as for the detector noise but with $a = \exp(-k\Delta t/2)$ and σ^2 is the signal variance at the beginning of the decay. The predicted limiting noise for a single decay $\sigma_k^2 = k^3(h\nu/QI_{th})$. Based upon both the cavity excitation intensity versus excitation time and how the standard error for k rises as the fit interval is reduced, we find that the sensitivity is maximized if $I_{th} = 2.47I_0$ ($\langle\Delta t_{trig}\rangle = 6.01\tau$) and $N\Delta t = 5.67\tau$, giving an event trigger rate of $0.086\ k$ and noise of k per root Hz of $2.31k(h\nu/QI_0)^{1/2}$. This is the fifth row of Table 3. As shown in the last column of Table 3, this has an overall $k^{1/2}$ dependence, and thus for sufficient input power for shot noise to dominate over detector noise, sensitivity increases with lower loss optical cavities even when the laser linewidth is much larger than the cavity width. If data set no. 8 were SNL and recorded with optimum trigger threshold $2.47I_0$, the initial S/N would be about 4100, and the optimized sensitivity would be $\alpha_{min} = 2.31k/c(h\nu/QI_0)^{1/2} = 1.6 \times 10^{-13}$ $cm^{-1}/(Hz^{1/2})$, which is about 50 times lower noise than our experimental value.

With $k = c(1-R)/L$, this optimized SNL sensitivity can be written down in another form

$$\alpha_{min} = 2.31\frac{1-R}{L}\sqrt{\frac{h\nu}{QI_0}} \tag{15}$$

with R the power reflectivity of mirror and L the cavity length. We can compare this optimized sensitivity with that of noise-immune cavity-enhanced optical heterodyne molecular spectroscopy (NICE–OHMS),[24] which has realized the highest sensitivity, 1×10^{-14} cm^{-1} in 1 s averaging time, among all laser based cavity-enhanced ultrasensitive methods. Its minimum detectable absorption is SNL, which is

$$\alpha_{min} = \frac{1}{\sqrt{2}J_0(\beta)J_1(\beta)}\frac{1-R}{L} \times \sqrt{\frac{2h\nu}{QP_0}} \xrightarrow{\beta=0.5} 4.4\ \frac{1-R}{L} \times \sqrt{\frac{h\nu}{QP_0}} \tag{16}$$

Here β is the modulation index, J_0 and J_1 are Bessel functions, and P_0 is the light power reaching the detector. Equation 16 is very similar to eq 15, meaning that in principle, both NICE–OHMS and cw-CRDS can reach the same high level of sensitivity. In their NICE–OHMS experiments, Ye et al.[24] realized the above record sensitivity by increasing the detected light power to mW level by using Hz-level linewidth laser and laser-cavity locking, and by combining cavity enhancement and frequency modulation (FM) together such that measuring the absorption signal at FSR frequency (typically several hundreds of MHz), at which lasers often have only SNL intensity fluctuations. On the contrary, with a noisy laser (linewidth ~MHz), the averaged cavity transmission I_0 in cw-CRDS is only about μW (Table 2), and hence the ring-down event rate is much lower than the optimum rate; furthermore, because cw-CRDS measures decay transients in the time domain directly, low-frequency noise sources,for example, cavity vibration, can contaminate the ring-down signal. All of them lead to the short-term sensitivity of typical cw-CRDS method is more than 2

dx.doi.org/10.1021/jp406691e | J. Phys. Chem. A XXXX, XXX, XXX–XXX

orders of magnitude less than that of the best NICE−OHMS sensitivity.[24]

Recently, the sensitivity of cw-CRDS method has been improved substantially by employing new experimental techniques. In a method called saturated absorption cavity ring-down spectroscopy (SCAR),[25] different from traditional exponential decay transients, the initial part of SCAR transients is saturated because of large intracavity light intensity, which decays approximately as the empty cavity loss rate. Therefore, SCAR can measure the empty cavity loss rate and intracavity absorption signal simultaneously in a single decay transient and hence can improve the sensitivity by reducing the effect of background fluctuations. With their ultrastable cw-CRDS setup and having not reached its stability limit, Kassi and Campargue[26] have reached a final sensitivity of 5×10^{-13} cm^{-1} by averaging more than 6000 spectra which were continuously recorded in 4.5 days at a ring-down event rate of 30 Hz. The sensitivity was demonstrated by measuring the extremely weak S4 (3−0) electric quadrupole transition (1×10^{-31} cm/molecule) of N_2 near 6945 cm^{-1}. The ring-down signal in their experiment is mainly DNL. Truong et al.[27] developed a new version of cw-CRDS: frequency-agile, rapid scanning (FARS) CRDS, in which the laser frequency is step-scanned accurately by a large bandwidth EOM to realize successive resonance between the laser and different cavity TEM_{00} modes in a very rapid speed. With narrow linewidth fiber laser (<100 Hz) and with an external-cavity diode laser (ECDL) (≤200 kHz), they have obtained a ring-down event rate of 8 kHz (limited by ring-down time τ only) and reached a sensitivity of $\sim 2 \times 10^{-12}$ cm^{-1} $Hz^{-1/2}$ and with an impressive tuning range more than 70 GHz in 2 s.[27,28] The authors even demonstrated FARS-CRDS with a low-cost DFB laser but with less sensitivity.[27] The sensitivity of FARS-CRDS has surpassed that of recent fiber-laser based NICE−OHMS.[29]

We will now consider FARS-CRDS and other experiments with an incident laser that has a very narrow linewidth compared to the cavity mode linewidth (i.e., $\Delta\nu_L \ll 1/2\pi\tau = \Delta\nu_c$) and is tightly locked to the cavity mode. Beginning from an optically empty cavity, the transmitted light intensity after turning on the excitation will ring-up as $I_0(1 - \exp(-kt/2))^2$,[30] with $I_0 = (T/(1 - R))^2 I_L$ the mean transmitted power. Under the above condition, there is no dead time between successive ring-up and ring-down transients.[28,30] Given the high transmitted power, we will assume that the ring-down transients are shot noise limited. Optimizing the trigger level and the detection interval, we predict shot-noise limited sensitivity of FARS-CRDS to be $\sigma_k = 3.77k(h\nu/QI_0)^{1/2}$, with trigger threshold $I_{th} = 0.831I_0$ (build-up time = 4.86τ), fitting interval $N\Delta t = 5.49\tau$ and ring-down event rate $0.0967k$. This result is included in the last row of Table 3, and it is proportional to k. With $\tau = 16$ μs, $\lambda = 1.5$ μm, and $Q = 0.8$, and assuming $I_0 = 1$ mW, the optimized SNL sensitivity gives a minimum detectable absorption of $\alpha_{min} = 1.0 \times 10^{-13}$ cm^{-1} $Hz^{-1/2}$. In their first FARS-CRDS experiments,[28] Long et al. obtained a sensitivity of 1.7×10^{-12} cm^{-1} $Hz^{-1/2}$. With $\tau = 220$ μs, as for our cavity, α_{min} will be 7.4×10^{-15} cm^{-1} $Hz^{-1/2}$, similar to the best reported NICE−OHMS sensitivity.[24] For completeness, we have included the optimum sensitivity for the case of SNL and $\Delta\nu_L \approx \Delta\nu_c$ into the sixth row of Table 3. When $\Delta\nu_L \approx \Delta\nu_c$ and upon turning on the excitation laser, by numerical simulation, the intracavity optical field increases steadily, and after the initial transient period ($\sim 10\tau$), the cavity output power fluctuation near the mean value I_0 is much smaller when compared with the case of $\Delta\nu_L \gg \Delta\nu_c$. This is true for both DNL and SNL cases.

In most practical cw-CRDS experiments, both the laser and the cavity drift and must be brought into resonance. One common approach is to sweep the laser or cavity slightly more than one free spectral range which insures that cavity and laser will pass through resonance at least once in each sweep. However, this reduces the time that one excites the cavity by a factor on the order of the laser linewidth divided by the cavity FSR, a factor ∼0.01−0.001 in many experiments. Furthermore, unless the sweep rate is such that the time to go through resonance (the laser width divided by the sweep rate, s in Hz/s) is longer than a few cavity τ, the excitation of the cavity will be reduced.[9] We have recently provided a thorough analysis of cavity excitation by a frequency swept cavity or laser, including providing expressions to the change in mean cavity transmission as a function of swept rate.[22] Experimentally, we have found that one can sweep by only $\sim D$ around the cavity resonance with modest loss in trigger rate over that when the laser is manually tuned onto resonance. The ramp voltage at which ring-down triggers occur is then sent back to the laser current or cavity PZT amplifier to maintain long-term locking of the laser and cavity. This allows detection of ring-down events at a rate near the above prediction.

CONCLUSION

In this article, we first briefly introduced an optimized nonlinear LSF algorithm for data processing in CRDS experiments. This algorithm utilizes the fact that in the process of minimizing the χ^2 of the LSF to a single exponential function, simple closed form expressions for the fit curvature matrix can be given when the decay transients are sampled evenly in time and either detector or shot noise dominates. Due to this fact, the optimized algorithm is more efficient in calculation than many other noniterative fitting algorithms. From the analytical form of matrix α, we have derived theoretical sensitivity limits from a single decay transient for both the DNL and the SNL cases. Data correlation caused by necessary filtering is also considered and can be included by a scale factor $G > 1$. We believe these results are instructive for designing and performing CRDS based experiments. Our model results are compared with experimental cw-CRDS results using a well characterized instrument. We found our model reproduces many of the experimental results very well, though it does underestimate the observed shot-to-shot variations in the cavity decay rate. Specifically, we demonstrated the effectiveness of correction factor G, and compared the predicted variances of k from rigorous covariance matrix with theoretical limits of DNL and SNL cases. As an approximation, the direct sum of the DNL and SNL variances works well only near DNL side and is about 50% less than the correct value near the SNL end. When shot noise is included in LSF, the correct definition of reduced χ^2 must include a weight of both noises for each data point of a transient. If ring-down transients are mainly detector noise limited, the effect of shot noise correlation is minor.

Based on the analytical form of the optimized LSF and numerical simulations, we have determined the optimal trigger level I_{th} and the length of fitting window of cw-CRDS for both DNL and SNL cases when the cavity is excited by a noisy laser. This optimization gives the highest sensitivities for both conditions. In our experiments, the sensitivity from a single decay transient is about several times lower than the predicted single shot limit, while the measured sensitivity per unit

dx.doi.org/10.1021/jp406691e | J. Phys. Chem. A XXXX, XXX, XXX−XXX

bandwidth, in cm^{-1} $Hz^{-1/2}$, is more than 1 order of magnitude lower than the optimized highest sensitivity under the same experimental conditions because of much lower trigger threshold and ring-down event rate than optimum ones. Interestingly, the expression of the optimized shot noise limitation on cw-CRDS sensitivity is very close to that of NICE−OHMS, suggesting that the principle difference in their observed sensitivities are due to technical limitations, principally the much larger bandwidth of the lasers that have primarily been used for cw-CRDS experiments, which reduces the mean optical transmission of the cavity.

AUTHOR INFORMATION

Corresponding Author

*E-mail: lehmann@virginia.edu.

Notes

The authors declare no competing financial interest.

ACKNOWLEDGMENTS

This work is supported by the National Science Foundation and by the University of Virginia. The authors thank Ray McIntyre of Tiger Optics for helpful discussions on the noise analysis of amplifiers with transimpedance design, thank Dr. David L. Osborn for letting H. Huang use the HP spectral analyzer, and thank Dr. Joseph T. Hodges for reading the manuscript carefully before its publication.

REFERENCES

(1) Scherer, J. J.; Paul, J. B.; Collier, C. P.; O'Keefe, A.; Rakestraw, D. J.; Saykally, R. J. Cavity ringdown laser spectroscopy: A new ultrasensitive absorption technique. *Spectroscopy* **1996**, *11*, 46−50.

(2) Busch, K. W., Busch, M. A., Eds. *Cavity Ringdown Spectroscopy: An Ultratrace-Absorption Measurement Technique*; ACS Symposium Series 720; American Chemical Society: Washington, DC, 1999.

(3) Berden, G.; Peeters, R.; Meijer, G. Cavity ring-down spectroscopy: Experimental schemes and applications. *Int. Rev. Phys. Chem.* **2000**, *19*, 565−607.

(4) Vallance, C. Innovations in cavity ringdown spectroscopy. *New J. Chem.* **2005**, *29*, 867−874.

(5) Long, D. A.; Havey, D. K.; Okumura, M.; Pickett, H. M.; Miller, C. E.; Hodges, J. T. Laboratory measurements and theoretical calculations of O_2 *A* band electric quadrupole transitions. *Phys. Rev. A* **2009**, *80*, 042513.

(6) O'Keefe, A.; Deacon, D. A. G. Cavity ring-down optical spectrometer for absorption measurements using pulsed laser sources. *Rev. Sci. Instrum.* **1988**, *59*, 2544−2551.

(7) Romanini, D.; Lehmann, K. K. Ring-down cavity absorption spectroscopy of the very weak HCN overtone bands with six, seven, and eight stretching quanta. *J. Chem. Phys.* **1993**, *99*, 6287−6301.

(8) Lehmann, K. K.; Huang, H. Optimal Signal Processing in Cavity Ring-Down Spectroscopy. In *Frontiers of Molecular Spectroscopy*; Laane, J., Ed.; Elsevier: Amsterdam, 2008; Chapter 18, pp 623−658.

(9) Huang, H.; Lehmann, K. K. Noise caused by a finite extinction ratio of the light modulator in cw cavity ring-down spectroscopy. *Appl. Phys. B: Laser Opt.* **2009**, *94*, 355−366.

(10) Press, W. H.; Flannery, B. P.; Teukolsky, S. A.; Vetterling, W. T. *Numerical Recipes in C: The Art of Scientific Computing*, 2nd ed.; Cambridge University Press: New York, 1992.

(11) Mazurenka, M.; Wada, R.; Shillings, A. J. L.; Butler, T. J. A.; Beames, J. M.; Orr-Ewing, A. J. Fast Fourier transform analysis in cavity ring-down spectroscopy: application to an optical detector for atmospheric NO_2. *Appl. Phys. B: Laser Opt.* **2005**, *81*, 135−141.

(12) Matheson, I. B. C. The Method of Successive Integration - A general technique for recasting kinetic-equations in a readily soluble form which is linear in the coefficients and sufficiently rapid for real-time instrumental use. *Anal. Instrum.* **1987**, *16*, 345.

(13) Halmer, D.; von Basum, G.; Hering, P.; Murtz, M. Fast exponential fitting algorithm for real-time instrument use. *Rev. Sci. Instrum.* **2004**, *75*, 2187−2191.

(14) Engeln, R.; von Helden, G.; Berden, G.; Meijer, G. Phase shift cavity ring down absorption spectroscopy. *Chem. Phys. Lett.* **1996**, *262*, 105−109.

(15) Spence, T. G.; Harb, C. C.; Paldus, B. A.; Zare, R. N.; Willke, B.; Byer, R. L. A laser-locked cavity ring-down spectrometer employing an analog detection scheme. *Rev. Sci. Instrum.* **2000**, *71*, 347−353.

(16) Huang, H.; Lehmann, K. K. Noise in cavity ring-down spectroscopy caused by transverse mode coupling. *Opt. Express* **2007**, *15*, 8745−8759.

(17) Chiu, Y.-J.; Fleischer, S. B.; Lasaosa, D.; Bowers, J. E. Ultrafast (370 GHz bandwidth) p-i-n traveling wave photodetector using low-temperature-grown GaAs. *Appl. Phys. Lett.* **1997**, *71*, 2508−2510.

(18) *Transimpedance Considerations for High-Speed Amplifiers*; Texas Instruments Application Report SBOA122; Texas Instruments: Dallas, TX, 2009.

(19) Huang, H.; Lehmann, K. K. Long-term stability in continuous wave cavity ringdown spectroscopy experiments. *Appl. Opt.* **2010**, *49*, 1378−1387.

(20) Huang, H.; Lehmann, K. K. CW cavity ring-down spectroscopy (CRDS) with a semiconductor optical amplifier as intensity modulator. *Chem. Phys. Lett.* **2008**, *463*, 246−250.

(21) Dudek, J. B.; Tarsa, P. B.; Velasquez, A.; Wladyslawski, M.; Rabinowitz, P.; Lehmann, K. K. Trace moisture detection using continuous-wave cavity ring-down spectroscopy. *Anal. Chem.* **2003**, *75*, 4599−4605.

(22) Huang, H.; Lehmann, K. K. Sensitivity Limit of Rapidly Swept Continuous Wave Cavity Ring-Down Spectroscopy. *J. Phys. Chem. A* **2011**, *115*, 9411−9421.

(23) Morville, J.; Romanini, D.; Chenevier, M.; Kachanov, A. A. Effects of laser phase noise on the injection of a high-finesse cavity. *Appl. Opt.* **2002**, *41*, 6980−6990.

(24) Ye, J.; Ma, L.-S.; Hall, J. L. Ultrasensitive detections in atomic and molecular physics: demonstration in molecular overtone spectroscopy. *J. Opt. Soc. Am. B* **1998**, *15*, 6−15.

(25) Giusfredi, G.; Bartalini, S.; Borri, S.; Cancio, P.; Galli, I.; Mazzotti, D.; Natale, P. D. Saturated-Absorption Cavity Ring-Down Spectroscopy. *Phys. Rev. Lett.* **2010**, *104*, 110801.

(26) Kassi, S.; Campargue, A. Cavity ring down spectroscopy with 5 × 10^{-13} cm^{-1} sensitivity. *J. Chem. Phys.* **2012**, *137*, 234201.

(27) Truong, G.-W.; Douglass, K. O.; Maxwell1, S. E.; van Zee, R. D.; Plusquellic, D. F.; Hodges, J. T.; Long, D. A. Frequency-agile, rapid scanning spectroscopy. *Nat. Photonics* **2013**, *7*, 532−534.

(28) Long, D. A.; Truong, G.-W.; van Zee, R. D.; Plusquellic, D. F.; Hodges, J. T. Frequency-agile, rapid scanning spectroscopy: Absorption sensitivity of 2 × 10^{-12} cm^{-1} $Hz^{-1/2}$ with a tunable diode laser. *Appl. Phys. B: Laser Opt.* **2013**, DOI 10.1007/s00340-013-5548-5.

(29) Ehlers, P.; Silander, I.; Wang, J.; Axner, O. Fiber-laser-based noise-immune cavity-enhanced optical heterodyne molecular spectrometry instrumentation for Doppler-broadened detection in the 10^{-12} cm^{-1} $Hz^{-1/2}$ region. *J. Opt. Soc. Am. B* **2012**, *29*, 1305−1315.

(30) Ye, J.; Hall, J. L. Cavity ringdown heterodyne spectroscopy: High sensitivity with microwatt light power. *Phys. Rev. A* **2000**, *61*, 061802.